ARTICLE IN PRESS

Communications Biology

https://doi.org/10.1038/s42003-026-09951-x

Article in Press

Quantitative comparison of methods for widespread delivery of small molecules across the blood-brain barrier

Received: 6 August 2025

Accepted: 18 March 2026

Cite this article as: Dawson, M., Bricault, S., Harvey, P. *et al.* Quantitative comparison of methods for widespread delivery of small molecules across the blood-brain barrier. *Commun Biol* (2026). https://doi.org/10.1038/s42003-026-09951-x

Miranda Dawson, Sarah Bricault, Peter Harvey, Agata Wisniowska, He Wei, Xun Wang, Gracia García-García, Takashi Kaise, Roger D. Kamm & Alan Jasanoff

We are providing an unedited version of this manuscript to give early access to its findings. Before final publication, the manuscript will undergo further editing. Please note there may be errors present which affect the content, and all legal disclaimers apply.

If this paper is publishing under a Transparent Peer Review model then Peer Review reports will publish with the final article.

ARTICLE IN PRESS

© The Author(s) 2026. **Open Access** This article is licensed under a Creative Commons Attribution-NonCommercial-NoDerivatives 4.0 International License, which permits any non-commercial use, sharing, distribution and reproduction in any medium or format, as long as you give appropriate credit to the original author(s) and the source, provide a link to the Creative Commons licence, and indicate if you modified the licensed material. You do not have permission under this licence to share adapted material derived from this article or parts of it. The images or other third party material in this article are included in the article's Creative Commons licence, unless indicated otherwise in a credit line to the material. If material is not included in the article's Creative Commons licence and your intended use is not permitted by statutory regulation or exceeds the permitted use, you will need to obtain permission directly from the copyright holder. To view a copy of this licence, visit http://creativecommons.org/licenses/by-nc-nd/4.0/.

ARTICLE IN PRESS

Quantitative comparison of methods for widespread delivery of small molecules across the blood-brain barrier

Miranda Dawson[1*], Sarah Bricault[1*], Peter Harvey[1*†], Agata Wisniowska[2], He Wei[1], Xun Wang[1], Gracia García-García[1], Takashi Kaise[1], Roger D. Kamm[1,3], & Alan Jasanoff[1,4,5‡]

[1] Department of Biological Engineering, Massachusetts Institute of Technology, 77 Massachusetts Ave., Cambridge, MA 02139, USA
[2] Harvard-MIT Health Sciences & Technology, Massachusetts Institute of Technology, 77 Massachusetts Ave., Cambridge, MA 02139, USA
[3] Department of Mechanical Engineering, Massachusetts Institute of Technology, 77 Massachusetts Ave., Cambridge, MA 02139, USA
[4] Department of Brain & Cognitive Sciences, Massachusetts Institute of Technology, 77 Massachusetts Ave., Cambridge, MA 02139, USA
[5] McGovern Institute for Brain Research, Massachusetts Institute of Technology, 43 Vassar St., Cambridge, MA 02139, USA

* These authors contributed equally to this work

† Present address: Sir Peter Mansfield Imaging Centre, School of Medicine & School of Chemistry, University of Nottingham, University Park, Nottingham NG7 2RD, UK

‡ Correspondence and requests for materials should be addressed to AJ (e-mail: *jasanoff@mit.edu*)

ARTICLE IN PRESS

Abbreviations: Blood-Brain Barrier (BBB), Brainstem (BS), Cerebellum (Cb), Cerebrospinal Fluid (CSF), Corpus Callosum (cc), Cortex (Cx), Dorsal Striatum (dSt), Hippocampus (Hi), Hypothalamus (HT), Longitudinal Relaxation Rate (R_1), Longitudinal Relaxation Time (T_1), Lysophosphatidic Acid (LPA), Magnetic Resonance Imaging (MRI), Midbrain (MB), Pearson's Correlation Coefficient (CC), Region of Interest (ROI), Thalamus (Th), Tomato Lectin (TL), Ultrasound (US), Ventral Striatum (vSt), Whole Brain (WB)

ARTICLE IN PRESS

ABSTRACT

Achieving widespread delivery of pharmacological agents beyond the blood-brain barrier (BBB) remains a formidable challenge in preclinical and clinical research. Here we quantitatively evaluate and compare three strategies for brain-wide delivery that employ transient BBB disruption or infusion via the cerebrospinal fluid (CSF) in rats. Using molecular magnetic resonance imaging (MRI) techniques, we find that the three techniques produce spatially differentiated labeling patterns, with the most homogeneous delivery produced either using chemically mediated or unfocused ultrasound-based BBB manipulation methods. Contrast enhancement distributions are similar following chemical and ultrasound procedures, but differ notably from the results of intra-CSF infusion. Delivery efficiency using the two BBB disruption methods also correlates inversely with a marker of tight junction density, suggesting that common factors determine susceptibility to these techniques. Our study thus documents the spatial variation of BBB properties across the brain while offering guidance about brain-wide application of molecular technologies in neuroscience and neuromedicine.

ARTICLE IN PRESS

INTRODUCTION

The blood-brain barrier (BBB) shields the brain from harmful and helpful substances alike[1, 2]. Although the barrier protects effectively against many toxins and infectious agents, it also bars entry to most drugs, complicating the treatment of disorders such as brain cancer, neuroinflammatory conditions, and neurological conditions[3]. By some accounts, only 2% of small-molecule therapeutics effectively cross the BBB on their own[4]. Tools of modern biomedicine, including engineered proteins, nanoparticles, and cells, are even more likely to be hindered because of their larger sizes. Important reagents in basic science, such as chemical actuators, imaging probes, and viral

ARTICLE IN PRESS

vectors, are also blocked, complicating fundamental investigations of brain biology. In some cases, reagents have been engineered to undergo spontaneous BBB permeation, for instance by conjugating them to substrates of receptor-mediated transcytosis across the BBB[5, 6]. Approaches that target the transferrin receptor have shown particular success in rodent and non-human primate models, and are now undergoing clinical trials[7-10]. These strategies require macromolecular modification of each substance to be delivered, however, and they are best suited for brain delivery of large biologic agents. Discovering and characterizing generalizable, minimally disruptive ways to bypass the BBB therefore remains an outstanding challenge in biomedical research.

Several techniques have emerged for widespread brain delivery of BBB-impermeant substances without the need for cranial surgery. These methods are considerably less invasive than intracranial infusion and may be useful in both laboratory and medical settings. Introduction of chemicals into accessible reservoirs of cerebrospinal fluid (CSF) has long been used to bypass the BBB[11], and animal studies of CSF flow profiles have shown that infusion into specific fluid chambers can enable injected agents to reach many areas of the brain[12, 13]. Substances introduced via the CSF are trafficked through the ventricles and along perivascular spaces by pulsatile and ciliary forces, in conjunction with pressure fields, before diffusing into the interstitial fluid of the parenchyma[11, 14, 15]. Transport within the parenchyma itself is governed by molecular size-dependent diffusive and convective factors that together determine spreading and clearance from the brain[16, 17]. Physical disruption of the BBB using low frequency (≤ 2 MHz) transcranial focused ultrasound (US) has been used to permit substances to enter the brain from the vasculature with spatial selectivity suitable for preclinical and clinical applications[18, 19], and a small number of studies have shown that unfocused US can also facilitate delivery to large brain areas in small animals[20-22]. Several decades after early demonstrations of this approach[23, 24], US methods are gaining clinical

ARTICLE IN PRESS

ARTICLE IN PRESS

momentum through trials in multiple brain disorders[25-28], where intravascular therapeutics are directed by localized BBB disruption to specific sites of action. Finally, chemically induced BBB disruption techniques have also shown promise for delivery of agents from the vasculature[29]. Delivery of small molecules and nanoparticles has been demonstrated using a specific approach in which BBB disruption is promoted by intravenous infusion of lysophosphatidic acid (LPA)[30, 31], an approach that parallels effects of clinically applied hyperosmotic BBB disruption methods[32].

To decide how to choose and use methods for widespread brain delivery of small molecules, it is important to understand how these techniques compare under analogous situations. How do CSF delivery or BBB disruption techniques perform under matched conditions in which the same molecule is delivered using each modality? Are there areas of the brain that are accessed preferentially by one delivery method or another? How does the time dependence of labeling and washout compare among the methods? Can regional or technique-dependent differences in trans-BBB delivery performance be understood mechanistically? Here we address these questions by combining brain administration methods with noninvasive molecular imaging in rodents. Quantitative comparison of the brain-wide delivery techniques using consistent experimental parameters identifies practical strengths and weaknesses of each technique, complementing earlier studies of each technique on its own and indicating approaches that could provide optimal utility for numerous contexts in basic and preclinical neuroscience research.

ARTICLE IN PRESS

RESULTS

Paradigms for widespread delivery of a small molecule contrast agent

To compare delivery strategies, we assessed the ability of each method to achieve brain-wide distributions of gadoteridol, a small (559 Da), neutral gadolinium complex that causes brightening

ARTICLE IN PRESS

in longitudinal relaxation time (T_1)-weighted magnetic resonance imaging (MRI)[33]. We measured gadoteridol-induced contrast changes using *in vivo* MRI of Sprague-Dawley rats, following four treatments (**Figure 1a,b**): (1) intracarotid delivery without BBB disruption (a negative control); (2) intravenous delivery via the tail vein, in conjunction with microbubble-assisted US-mediated BBB disruption using a 2.5 cm-diameter unfocused transducer; (3) intracarotid delivery with chemically mediated BBB disruption using coinfusion of 2 mg/kg LPA; and (4) intra-CSF delivery via infusion into the cisterna magna, a CSF reservoir that has been shown to facilitate brain-wide spread of injected substances. For the peripheral delivery treatments (1-3), a 1 mL dose of 500 mM gadoteridol was injected intravascularly. For the intra-CSF method (4) a 100 µL dose of 25 mM contrast agent was administered, under the supposition that dilution of this amount throughout ~2 mL brain tissue would produce roughly the same final concentration as present in blood after the intravascular injections[34, 35]. To minimize confounding effects from an increase in intracranial pressure during these intra-CSF injections[36], at least 200 µL of endogenous CSF was passively drained immediately prior to injection of the contrast agent.

ARTICLE IN PRESS

MRI results from parasagittal and coronal slices show that all the treatments, except the negative control, produce strong T_1-weighted signal enhancements in the brain, reflective of substantial gadoteridol delivery to representative animals. The bases of these image effects are quantitatively indicated by maps of the longitudinal relaxation rate R_1 (= $1/T_1$), a physical parameter that determines T_1 contrast and varies linearly with the gadoteridol concentration by a factor of 3.2 $mM^{-1}s^{-1}$ at 37 °C and 7 T[37]. Differences in R_1 over measured baseline values of about 0.43 s^{-1} in untreated control rat brains indicate that all three delivery techniques produce widespread effects corresponding to gadoteridol concentrations of up to ~0.8 mM (**Figure 1c**). The LPA technique also produced R_1 increases when applied via tail vein injection (**Supplementary Figure 1**), but

ARTICLE IN PRESS

this was less effective than the intracarotid route; no difference in brain contrast enhancement was observed between intracarotid and tail vein injection of gadoteridol in the absence of LPA.

For each delivery technique, relaxation rate changes could be further quantified by examining histograms of R_1 values obtained from multiple animals per condition (**Figure 1d**). Average relaxation rates measured from control animals after contrast agent injection were $0.51 \pm 0.004\ s^{-1}$, whereas values measured from US, and LPA, and CSF animals were $1.03 \pm 0.05\ s^{-1}$ ($n = 3$), $1.32 \pm 0.14\ s^{-1}$ ($n = 5$), and $0.97 \pm 0.08\ s^{-1}$ ($n = 4$), respectively. A large proportion of voxels in the three delivery conditions displayed R_1 values more than two standard deviations above the mean R_1 for the control condition: 60% for US, 76% for LPA, and 49% for CSF techniques. These results indicate that trans-BBB and intra-CSF delivery schemes were all highly effective at spreading gadoteridol over large volumes of brain tissue.

ARTICLE IN PRESS

Quantification of spatial aspects of brain delivery

Although each of the three tested methods successfully achieved widespread brain delivery of gadoteridol, the maps of **Figure 1** clearly show that there is spatial heterogeneity of the resulting R_1 enhancements. We sought to characterize this heterogeneity and determine its reproducibility. Mean and standard deviation maps depicting changes in R_1 were obtained from animals following US-mediated, LPA-mediated, and intra-CSF delivery of gadoteridol (**Figure 2a**). Results indicate that US-mediated delivery accesses tissue fairly homogeneously in a swath of tissue of ~8 mm, centered under the transducer, that likely reflects dimensions of the pressure field[20]; this could be extended by applying multiple sonications (**Supplementary Figure 2**). LPA-assisted delivery produces more homogeneous delivery along the rostrocaudal axis, but with a left-right asymmetry resulting from unilateral infusion through the carotid artery (**Supplementary Figure 3**). Intra-CSF

ARTICLE IN PRESS

delivery is less homogeneous, tending to reach ventral areas and regions close to the ventricles and cisterns for which the partial volume of CSF might be high[13]. In our hands, the most reproducible results were obtained using the US technique, as indicated by the low standard deviations of R_1 throughout the sagittal section analyzed. Although LPA results were more variable, normalization of R_1 changes by the brain-wide average values after LPA-mediated delivery substantially narrowed the distribution of ROI results (**Supplementary Figure 4**), suggesting that relative susceptibility of ROIs to chemical disruption was largely conserved across animals.

To form a more systematic impression of delivery efficacy to different brain areas, we analyzed gadoteridol-mediated R_1 enhancements over regions of interest (ROIs) based on a standard brain atlas[38] (**Figure 2b**). Mean changes in R_1 from baseline (ΔR_1 values) varied by up to 5-fold (US), 3-fold (LPA), or 26-fold (CSF) over the different ROIs (**Figure 2c**). The hypothalamus (HT) experienced particularly effective delivery using all three techniques, possibly reflecting its proximity to the subfornical organ and the median eminence, both circumventricular regions that lack a fully formed BBB[39]. In contrast, the cerebellum was poorly accessed by all of the methods. Quantitative comparison of ROI-level delivery results (**Figure 2d**) showed very close correspondence between average ΔR_1 values obtained using the US and LPA techniques (Pearson's correlation coefficient, CC = 0.97, $p < 10^{-4}$, $n = 10$ ROIs); this correlation persisted even when caudal cerebellar and brainstem regions that were not well addressed by the US transducer were excluded (CC = 0.93, $p = 0.0008$, $n = 8$). Much looser correspondence was observed between intra-CSF infusion and LPA-mediated delivery (CC = –0.15, $p = 0.67$, $n = 10$), however (**Figure 2e**), and the comparison between CSF infusion and US-mediated delivery (**Supplementary Figure 5**) was similarly weak (CC = –0.16, $p = 0.66$).

ARTICLE IN PRESS

ARTICLE IN PRESS

Kinetic analysis of contrast agent transport after delivery

Contrast changes induced by US-mediated, LPA-assisted, and CSF infusion-based gadoteridol delivery using the procedures of **Figure 1** were measured over a period of 100-200 minutes following each procedure, raising the possibility of comparing the dynamics of molecular delivery using each approach. US-treated animals were followed for a shorter period than other techniques due to the complexity of the experimental setup and length of anesthesia required. Peak delivery times and initial wash-out stages were captured for all three delivery methods, however, enabling quantitative comparisons of information present in the corresponding R_1 time series. Despite stark differences in the nature and timing of the delivery protocols, all three methods resulted in brain-wide MRI signal increases that peaked on the order of an hour after the delivery treatment (**Figure 3a**). Similar temporal profiles were observed within individual ROIs as well (**Supplementary Figure 6**). Mean times to peak were 31 ± 9 min for US, 27 ± 5 min for LPA, and 66 ± 4 min for CSF delivery (**Figure 3b**), indicating that gadoteridol continued to enter the brain or spread from initial sites of entry for many minutes following each procedure.

To analyze this process more precisely, we fit the time series at each voxel to a linear two-compartment kinetic model in which all sources of out-of-voxel gadoteridol were lumped into one compartment and the within-voxel contrast was represented by the second compartment. The time course of relaxivity change predicted in this scenario is given by:

$$\Delta R_1 = \frac{c}{k_{out} - k_{in}} \left(e^{-k_{in} t} - e^{-k_{out} t} \right) \quad (1)$$

where the rate constant k_{in} describes influx of agent into a voxel, k_{out} describes efflux, and c is a scaling constant. Data from each voxel exhibiting substantial R_1 changes were fit to Eq. 1, yielding parameter estimates from 67%, 99%, and 57% voxels across 3-5 animals in the US, LPA, and CSF

ARTICLE IN PRESS

delivery conditions, respectively (**Figure 3c**). Average fitted values of k_{out} and k_{in} are diagrammed in **Figure 3d** and **Supplementary Figure 7**.

Values of k_{out} in particular reflect dissipation of contrast agent after each delivery procedure is largely completed, so we surmised that these rate constants might reflect consistent properties of small molecule transport in the brain. Indeed, mean k_{out} values do fall in a relatively uniform range, with brain-wide averages of 7.8 ± 0.9, 9.3 ± 2.5, and $9.3 \pm 1.1 \times 10^{-3}$ s^{-1} for US, LPA, and CSF delivery data, respectively. Nevertheless, when compared among ROIs (**Figure 3e**), some regional variability among k_{out} values is apparent following each method of brain delivery. Comparison of mean washout rates from regions that received substantial delivery also reveals systematic differences between the techniques (**Figure 3f**). Observed k_{out} values for several regions were significantly higher after LPA-mediated delivery than after US (vSt, thalamus, HT; unpaired Student's t-test $p \leq 0.017$, $n = 3\text{-}4$) or CSF (vSt; t-test $p = 0.009$, $n = 3\text{-}4$) and and little overall correlation among the methods was seen ($p \geq 0.58$, $n = 5\text{-}9$ ROIs). These results suggest that aftereffects of the three delivery techniques disparately influence subsequent transport of administered substances.

Histological correlates of brain-wide delivery

The close correspondence of trans-BBB delivery profiles achieved following US and LPA treatments led us to ask whether specific tissue properties could account for the observed contrast distributions. We speculated that determinants could include the density of blood vessels, from which contrast agent enters the tissue in the presence of a compromised BBB, and the prevalence of tight junctions that promote BBB integrity and are disrupted by US[40] or LPA[41]. *In vitro* modeling[42] of the effects of LPA confirmed that this agent specifically alters vessel permeability at a

ARTICLE IN PRESS

microscopic level (**Supplementary Figure 8**), prompting us also to wonder whether LPA receptor distribution might help explain the spatial profile of LPA-dependent BBB opening at a macroscopic scale.

To examine the importance of these factors, we used histochemical labeling to visualize markers of vascular endothelial cells (reactivity with tomato lectin, TL), tight junctions (the protein ZO-1), and LPA sensitivity (the LPA receptor LPAR6) across sagittal brain slices approximately matched to the MRI geometry of Figs. 1-3 (**Figure 4a-c** and **Supplementary Figure 9**). All three markers stained with varying intensities across the field of view and could be quantified in maps and ROIs similar to those used to characterize contrast agent delivery parameters measured by MRI (**Figure 4d,e**). ROI-level comparison of the staining results with ΔR_1 measurements from **Figure 2** shows a diversity of correspondence between histology and contrast agent delivery (**Figure 4f**). TL and LPAR6 staining did not relate strongly to the MRI results, but staining for the ZO-1 tight junction protein displayed inverse correlations with the imaging data that were significant following US-mediated delivery (p = 0.02, n = 10 ROIs) and almost significant after LPA-mediated delivery (p = 0.07). This suggests that tight junction density contributes importantly to the efficacy of brain-wide trans-BBB delivery.

DISCUSSION

Achieving widespread delivery of chemicals to the brain is a major challenge in neuroscience and neuromedicine. Here we have used molecular MRI to assess the ability of three delivery techniques to enable a representative exogenous contrast agent to reach broad regions of brain tissue in rodents. We found that US- and LPA-mediated BBB disruption promote variegated but spatially similar profiles of delivery throughout cortical and subcortical areas. Conversely, CSF infusion

ARTICLE IN PRESS

via the cisterna magna produced less homogeneous distributions that were more pronounced around CSF reservoirs and ventral brain regions, consistent with previous reports[13, 43]. Analysis of MRI time courses following delivery showed that contrast changes peak about an hour after treatment with each method. Average washout rate constants of order 0.01 s^{-1} are observed for all brain regions, with modest treatment-dependent differences that may reflect aftereffects of each delivery approach. Some of our spatial results appeared to reflect the distribution of markers in brain vasculature, emphasizing the interaction of delivery parameters with physiological characteristics of the brain itself.

Each of the brain delivery methods we evaluated displayed pros and cons with respect to the others (**Figure 4g**). The US technique produced widespread and relatively stable contrast enhancement. Although it required specialized equipment and coinjection of microbubbles[44], results obtained with this approach were quite reproducible. Even using the 2.5 cm-diameter flat transducer we applied, the US technique could not produce uniform brain labeling, but we found that application of US treatment at four positions could largely address this limitation. The LPA-mediated delivery method was the easiest to implement in our hands. Results varied most among animals, even though a strictly controlled injection rate was implemented. Although the LPA technique as we applied it in rats involved preimplantation with a carotid catheter, the delivery procedure itself required just a single acute injection of LPA with gadoteridol via the catheter; we also showed that intravenous administration produces brain contrast enhancement, albeit more modestly. Intra-CSF delivery was the most invasive procedure and the least effective in reaching multiple brain areas, but it uses less of the injected substance and does not impinge on peripheral tissues and organs. A combination of the methods implemented here might be most effective at delivering substances

ARTICLE IN PRESS

ARTICLE IN PRESS

throughout the entire brain. In particular, the CSF method we used was comparatively adept at accessing caudal structures that the US and LPA methods addressed less successfully.

Our experiments did not attempt to characterize the time courses of BBB closure following disruption by LPA or US, but earlier reports have shown that both BBB opening techniques are reversible. Following focused US in rats, tight junctions have been shown to reform within about six hours[40], and LPA-mediated BBB disruption in mice appears to last less than 20 min[30]. We assume that BBB dynamics took place on similar time scales in our study, despite some differences in how we applied the techniques. A potential longer term consequence of BBB opening is the induction of inflammatory processes in the brain. Prior studies of US-mediated BBB disruption in rats have shown evidence of inflammation lasting for many hours following sonication under some parameter choices[45, 46]. To the extent that such effects are exacerbated by BBB opening itself, the LPA technique could likewise be susceptible, though the faster reversal of LPA-induced BBB disruption might provide an advantage over US in this regard. We controlled for some side-effects of BBB opening by monitoring physiology throughout our experiments, and we observed that animals maintained strong vital signs during imaging. We also examined T_2-weighted scans for evidence of microhemorrhages, but did not observe obvious lesions.

A limitation of our study is the fact that we had to make arbitrary choices about the way we implemented each of the delivery methods. This involved choosing timing, injection routes, concentrations, and other parameters for all techniques, plus apparatus for the US method. In addition, we performed all delivery experiments in rats, using a single molecule—the hydrophilic but neutral MRI contrast agent gadoteridol—as a delivery substrate. Although each of the methods we used is related to clinically applied approaches, they are likely to scale differently for brains and species of different size, with brain-wide distributions more difficult to achieve for larger brains due to

ARTICLE IN PRESS

transport issues, among other factors. Larger or more hydrophobic molecules will also be more difficult to deliver. Previous studies have shown that trans-BBB delivery of large agents results in much more restricted spread from vascular compartments[47-49]; the same consideration applies to spreading from the perivascular Virchow-Robin space following intra-CSF injection[36].

Two of our principal findings are likely to hold despite these concerns, however: first, the complementary characteristics of intra-CSF and trans-BBB molecular delivery profiles follow neuroanatomical features that are conserved across mammalian species and naturally independent of the delivered molecule. Complementarity of CSF and trans-BBB delivery profiles is therefore likely to persist across species and substrates. Second, spatial similarities we have documented between brain-wide US and LPA trans-BBB delivery profiles—which arise from very different mechanisms but both correlate somewhat negatively with a histological marker of tight junction density—suggest that specifics of how the protocols are implemented are less important than tissue properties in determining spatial contours of the delivery results. This conclusion may also apply to brain delivery methods untested in our experiments, such as techniques that employ osmotic disruption[32] or perhaps even receptor-mediated transport pathways[6]. The comparative study we present here may thus offer both a guide to applying the specific brain delivery techniques we assessed and a basis for anticipating results of delivery approaches that are yet to be investigated.

ARTICLE IN PRESS

REFERENCES

1. Abbott, N.J., Patabendige, A.A., Dolman, D.E., Yusof, S.R. & Begley, D.J. Structure and function of the blood-brain barrier. *Neurobiol Dis* **37**, 13-25 (2010).
2. Neuwelt, E.A. et al. Engaging neuroscience to advance translational research in brain barrier biology. *Nat Rev Neurosci* **12**, 169-182 (2011).

ARTICLE IN PRESS

3. Terstappen, G.C., Meyer, A.H., Bell, R.D. & Zhang, W. Strategies for delivering therapeutics across the blood-brain barrier. *Nat Rev Drug Discov* **20**, 362-383 (2021).
4. Pardridge, W.M. Treatment of Alzheimer's Disease and Blood-Brain Barrier Drug Delivery. *Pharmaceuticals (Basel)* **13** (2020).
5. Goulatis, L.I. & Shusta, E.V. Protein engineering approaches for regulating blood-brain barrier transcytosis. *Curr Opin Struct Biol* **45**, 109-115 (2017).
6. Pulgar, V.M. Transcytosis to Cross the Blood Brain Barrier, New Advancements and Challenges. *Front Neurosci* **12**, 1019 (2018).
7. Grimm, H.P. et al. Delivery of the Brainshuttle amyloid-beta antibody fusion trontinemab to non-human primate brain and projected efficacious dose regimens in humans. *MAbs* **15**, 2261509 (2023).
8. Barker, S.J. et al. Targeting the transferrin receptor to transport antisense oligonucleotides across the mammalian blood-brain barrier. *Sci Transl Med* **16**, eadi2245 (2024).
9. Huang, Q. et al. An AAV capsid reprogrammed to bind human transferrin receptor mediates brain-wide gene delivery. *Science* **384**, 1220-1227 (2024).
10. Khoury, N. et al. Fc-engineered large molecules targeting blood-brain barrier transferrin receptor and CD98hc have distinct central nervous system and peripheral biodistribution. *Nat Commun* **16**, 1822 (2025).
11. Sadekar, S.S. et al. Translational Approaches for Brain Delivery of Biologics via Cerebrospinal Fluid. *Clin Pharmacol Ther* **111**, 826-834 (2022).
12. Iliff, J.J. et al. A paravascular pathway facilitates CSF flow through the brain parenchyma and the clearance of interstitial solutes, including amyloid beta. *Sci Transl Med* **4**, 147ra111 (2012).

ARTICLE IN PRESS

ARTICLE IN PRESS

13. Iliff, J.J. et al. Brain-wide pathway for waste clearance captured by contrast-enhanced MRI. *J Clin Invest* **123**, 1299-1309 (2013).
14. Jessen, N.A., Munk, A.S., Lundgaard, I. & Nedergaard, M. The Glymphatic System: A Beginner's Guide. *Neurochem Res* **40**, 2583-2599 (2015).
15. Abbott, N.J., Pizzo, M.E., Preston, J.E., Janigro, D. & Thorne, R.G. The role of brain barriers in fluid movement in the CNS: is there a 'glymphatic' system? *Acta Neuropathol* **135**, 387-407 (2018).
16. Wolak, D.J. & Thorne, R.G. Diffusion of macromolecules in the brain: implications for drug delivery. *Mol Pharm* **10**, 1492-1504 (2013).
17. Nicholson, C. & Hrabetova, S. Brain Extracellular Space: The Final Frontier of Neuroscience. *Biophys J* **113**, 2133-2142 (2017).
18. Szablowski, J.O., Bar-Zion, A. & Shapiro, M.G. Achieving Spatial and Molecular Specificity with Ultrasound-Targeted Biomolecular Nanotherapeutics. *Acc Chem Res* **52**, 2427-2434 (2019).
19. McMahon, D., O'Reilly, M.A. & Hynynen, K. Therapeutic Agent Delivery Across the Blood-Brain Barrier Using Focused Ultrasound. *Annu Rev Biomed Eng* **23**, 89-113 (2021).
20. Howles, G.P. et al. Contrast-enhanced in vivo magnetic resonance microscopy of the mouse brain enabled by noninvasive opening of the blood-brain barrier with ultrasound. *Magn Reson Med* **64**, 995-1004 (2010).
21. McDannold, N., Zhang, Y. & Vykhodtseva, N. Blood-brain barrier disruption and vascular damage induced by ultrasound bursts combined with microbubbles can be influenced by choice of anesthesia protocol. *Ultrasound Med Biol* **37**, 1259-1270 (2011).

ARTICLE IN PRESS

ARTICLE IN PRESS

22. Beccaria, K. et al. Opening of the blood-brain barrier with an unfocused ultrasound device in rabbits. *J Neurosurg* **119**, 887-898 (2013).

23. Bakay, L., Ballantine, H.T., Jr., Hueter, T.F. & Sosa, D. Ultrasonically produced changes in the blood-brain barrier. *AMA Arch Neurol Psychiatry* **76**, 457-467 (1956).

24. Hynynen, K., McDannold, N., Vykhodtseva, N. & Jolesz, F.A. Noninvasive MR imaging-guided focal opening of the blood-brain barrier in rabbits. *Radiology* **220**, 640-646 (2001).

25. Lipsman, N. et al. Blood-brain barrier opening in Alzheimer's disease using MR-guided focused ultrasound. *Nat Commun* **9**, 2336 (2018).

26. Gasca-Salas, C. et al. Blood-brain barrier opening with focused ultrasound in Parkinson's disease dementia. *Nat Commun* **12**, 779 (2021).

27. Rezai, A.R. et al. Ultrasound Blood-Brain Barrier Opening and Aducanumab in Alzheimer's Disease. *N Engl J Med* **390**, 55-62 (2024).

28. Wu, C.C. et al. Blood-brain barrier opening with neuronavigation-guided focused ultrasound in pediatric patients with diffuse midline glioma. *Sci Transl Med* **17**, eadq6645 (2025).

29. Bhunia, S. et al. Drug Delivery to the Brain: Recent Advances and Unmet Challenges. *Pharmaceutics* **15** (2023).

30. On, N.H., Savant, S., Toews, M. & Miller, D.W. Rapid and reversible enhancement of blood-brain barrier permeability using lysophosphatidic acid. *J Cereb Blood Flow Metab* **33**, 1944-1954 (2013).

31. Sun, Z. et al. Biodistribution of negatively charged iron oxide nanoparticles (IONPs) in mice and enhanced brain delivery using lysophosphatidic acid (LPA). *Nanomedicine* **12**, 1775-1784 (2016).

ARTICLE IN PRESS

ARTICLE IN PRESS

32. Doolittle, N.D., Muldoon, L.L., Culp, A.Y. & Neuwelt, E.A. Delivery of chemotherapeutics across the blood-brain barrier: challenges and advances. *Adv Pharmacol* **71**, 203-243 (2014).

33. Tweedle, M.F. Physicochemical properties of gadoteridol and other magnetic resonance contrast agents. *Invest Radiol* **27 Suppl 1**, S2-6 (1992).

34. Probst, R.J. et al. Gender differences in the blood volume of conscious Sprague-Dawley rats. *J Am Assoc Lab Anim Sci* **45**, 49-52 (2006).

35. Westerhout, J., Ploeger, B., Smeets, J., Danhof, M. & de Lange, E.C. Physiologically based pharmacokinetic modeling to investigate regional brain distribution kinetics in rats. *AAPS J* **14**, 543-553 (2012).

36. Yang, L. et al. Evaluating glymphatic pathway function utilizing clinically relevant intrathecal infusion of CSF tracer. *J Transl Med* **11**, 107 (2013).

37. Szomolanyi, P. et al. Comparison of the Relaxivities of Macrocyclic Gadolinium-Based Contrast Agents in Human Plasma at 1.5, 3, and 7 T, and Blood at 3 T. *Invest Radiol* **54**, 559-564 (2019).

38. Paxinos, G. & Watson, C. The Rat Brain in Stereotaxic Coordinates, 7th Ed. (Academic Press, Boston; 2013).

39. Siso, S., Jeffrey, M. & Gonzalez, L. Sensory circumventricular organs in health and disease. *Acta Neuropathol* **120**, 689-705 (2010).

40. Sheikov, N., McDannold, N., Sharma, S. & Hynynen, K. Effect of focused ultrasound applied with an ultrasound contrast agent on the tight junctional integrity of the brain microvascular endothelium. *Ultrasound Med Biol* **34**, 1093-1104 (2008).

41. Schulze, C., Smales, C., Rubin, L.L. & Staddon, J.M. Lysophosphatidic acid increases tight junction permeability in cultured brain endothelial cells. *J Neurochem* **68**, 991-1000 (1997).

ARTICLE IN PRESS

ARTICLE IN PRESS

42. Pavlou, G. et al. Engineered 3D human neurovascular model of Alzheimer's disease to study vascular dysfunction. *Biomaterials* **314**, 122864 (2025).

43. Stanton, E.H. et al. Mapping of CSF transport using high spatiotemporal resolution dynamic contrast-enhanced MRI in mice: Effect of anesthesia. *Magn Reson Med* **85**, 3326-3342 (2021).

44. O'Reilly, M.A. & Hynynen, K. Ultrasound enhanced drug delivery to the brain and central nervous system. *Int J Hyperthermia* **28**, 386-396 (2012).

45. Kovacs, Z.I. et al. Disrupting the blood-brain barrier by focused ultrasound induces sterile inflammation. *Proc Natl Acad Sci U S A* **114**, E75-E84 (2017).

46. McMahon, D. & Hynynen, K. Acute Inflammatory Response Following Increased Blood-Brain Barrier Permeability Induced by Focused Ultrasound is Dependent on Microbubble Dose. *Theranostics* **7**, 3989-4000 (2017).

47. Choi, J.J., Wang, S., Tung, Y.S., Morrison, B., 3rd & Konofagou, E.E. Molecules of various pharmacologically-relevant sizes can cross the ultrasound-induced blood-brain barrier opening in vivo. *Ultrasound Med Biol* **36**, 58-67 (2010).

48. Blanchette, M., Tremblay, L., Lepage, M. & Fortin, D. Impact of drug size on brain tumor and brain parenchyma delivery after a blood-brain barrier disruption. *J Cereb Blood Flow Metab* **34**, 820-826 (2014).

49. Wei, H. et al. Single-nanometer iron oxide nanoparticles as tissue-permeable MRI contrast agents. *Proc Natl Acad Sci U S A* **118** (2021).

ARTICLE IN PRESS

ARTICLE IN PRESS

Acknowledgements

This research was funded by grants from the K. Lisa Yang Brain-Body Center and the NIH (U01 EB031641, R01 NS121073, R01 DA062195) to AJ. MD and SB were partially funded by the MIT Neurobiological Engineering Training Program (NIH T32 EB019940) and SB was also funded by a J. Douglas Tan Postdoctoral Fellowship from the McGovern Institute for Brain Research. PH was supported by a Wellcome Trust-MIT Postdoctoral Fellowship (105932/Z/14/Z). AW was partially funded by the Advanced Multimodal Neuroimaging Training Program at the Massachusetts General Hospital (NIH R90 DA023427). GGG was supported by a travel grant from the Universidad Francisco de Vitoria, and TK was funded by a JSPS Postdoctoral Fellowship for Research Abroad.

ARTICLE IN PRESS

Author contributions

MD, SB, and PH contributed equally. PH conceived the study. MD, SB, PH, AW, HW, and GGG performed experimental surgeries and imaging. MD and TK performed histology. MD and SB performed imaging analyses. XW and RDK developed and performed the microfluidic assay. MD and AJ wrote the paper with input from other authors. AJ supervised the research.

Competing interests

The authors declare no competing interests.

ARTICLE IN PRESS

METHODS

Animals

We have complied with all relevant ethical regulations for animal use. All animal procedures were performed in strict compliance with US Federal guidelines, with oversight by the MIT Committee on Animal Care, and in accordance with our approved animal protocol number 2404000655. Male Sprague-Dawley rats (150-300 g) were purchased from Charles River Laboratories (Wilmington, MA) and used for the *in vivo* data presented in this paper. Animals procured for LPA-mediated delivery were pre-implanted with chronic carotid artery catheters targeting the left side of the brain. Animals procured for intravenous administration were pre-implanted with tail-vein catheters. All animals were housed and maintained on a 12 h light/dark cycle with *ad libitum* access to food and water. During all imaging experiments, healthy physiology was ensured by monitoring heart rate and blood oxygen saturation, as well as maintaining core temperature with a circulating warm water pad (Gaymar, Orchard Park, NY) for the remainder of the procedure.

Chemicals

All chemicals were obtained from MilliporeSigma (Burlington, MA) unless otherwise noted. Gadoteridol contrast agent formulations used for all brain delivery experiments were obtained from Bracco (Milan, Italy). Optison microbubbles used in US-mediated delivery experiments were obtained from GE Healthcare (Chicago, IL).

Control delivery experiments

Four rats were used for negative control experiments. Animals were pre-implanted by the vendor (Charles River) with chronic carotid artery catheters targeting the left side of the brain. On the day of imaging, each rat was anesthetized with 3% isoflurane and its catheter clip was removed. Catheter patency was verified and animals with no backflow were excluded. The catheter was then connected to an injection line and the animal was moved to the scanner. Isoflurane was reduced to 1.5% for the remainder of the experiment. Animals were imaged immediately before and then for 1-3 h after a 1 mL intracarotid injection of 500 mM gadoteridol, delivered over approximately 17 s. A subset of these animals were briefly recovered following the procedure, and demonstrated normal behaviors. Pilot studies using higher injection rates demonstrated some contrast enhancement in control animals, presumably as a result of osmotic effects on the BBB.

ARTICLE IN PRESS

US-mediated brain delivery

Six rats were used for US-mediated brain delivery experiments. Animals were anesthetized with 2% isoflurane and then underwent the placement of the tail vein catheter for microbubble injection and contrast agent delivery. The tail vein was visualized by application of alcohol to the skin, and a catheter (24G Surflo, Terumo, Somerset, NJ) was slowly inserted into the vein until obvious blood back-flow was observed. The catheter was secured to the tail by placing a tongue depressor (Puritan, Guilford, ME) underneath the tail and taping the tail and the tongue depressor together using surgical tape. The catheter was flushed with 0.5% heparin in phosphate buffered saline (PBS) to prevent clotting and secured with a stopper prior to contrast agent infusion.

Animals subsequently underwent ultrasound-mediated BBB disruption. The rats were maintained under 2% isoflurane anesthesia. Heads were shaved and cleaned with alcohol and povidone-iodine prep pads for easy access to the skull. The skin over the skull was retracted and the skull cleaned to visualize the coronal and sagittal sutures. Ultrasound transmission gel (Parker

ARTICLE IN PRESS

Aquasonic, Fairfield, NJ) was applied to the exposed skull. An ultrasound transducer housing was then positioned in contact with the gel, with its center 1 mm above the skull, 3 mm lateral and 3 mm anterior to bregma. The housing was filled with circulating degassed and deionized water and was affixed to a custom transducer with 25 mm diameter and 500 kHz peak operating frequency (Sonic Concepts, Bothwell, WA). Ultrasound waveforms were generated using a 25 MHz function generator (BK Precision, Yorba Linda, CA) using the following settings: 500 kHz driving frequency, 0.2 V amplitude, 5,000 burst count, and 1 s burst rate. Waveforms were amplified using an ENI model 550L radiofrequency power amplifier (Bell Electronics, Renton, WA) conditioned through an impedance matching network (Sonic Concepts) connected to the transducer itself.

Sonication was applied to each animal, three rats received a single round of sonication and three received four sonications (3 mm bilaterally at 3 mm anterior or posterior to bregma). Each round of sonication lasted for 5 min. Immediately after the sonication was initiated, 50 µL of Optison microbubble ultrasound contrast agent (GE Healthcare, Chicago, IL) was injected through the tail vein catheter and flushed with 0.2 mL of 0.5% heparin in PBS. After sonication was completed, the skin was glued together using tissue glue and the animal was moved into the scanner. 1 mL of 500 mM gadoteridol was injected via the tail vein and imaging was performed for approximately 100 minutes after the injection. The duration of imaging was more limited than that applied for LPA and CSF delivery methods because of the longer pre-delivery anesthesia period required for set up and implementation of the US procedures we performed.

LPA-mediated brain delivery

LPA-mediated delivery procedures were applied to five rats. Animals were pre-implanted by the vendor (Charles River) with chronic carotid artery catheters targeting the left side of the brain. On the day of imaging, each rat was anesthetized with 3% isoflurane and its catheter clip was removed. Catheter patency was verified and animals no backflow were excluded. The catheter was then connected to an injection line and the animal was moved to the scanner. Isoflurane was reduced to 1.5% for the remainder of the experiment. Animals were imaged immediately before and then for 1-3 hours after a 1 mL carotid artery injection of 2 mg/kg LPA plus 500 mM gadoteridol, delivered over approximately 17 sec. A subset of these animals was briefly recovered following the procedure, and demonstrated normal behaviors.

LPA-mediated delivery was also performed via tail vein injection on three rats. Animals were anesthetized at 3% isoflurane and maintained at 1.5% for the rest of the experiment. Animals were then moved to the MRI cradle and implanted with a tail vein catheter that was then connected to an injection line. Animals were imaged before and then within 15 minutes after a 1 mL injection of 2 mg/kg LPA plus 500 mM gadoteridol, delivered over approximately 17 sec.

Intra-CSF injection

Intra-CSF delivery procedures were applied to four rats. All animals were imaged prior to the delivery procedure. Rats were anesthetized with 3% isoflurane and lidocaine was applied to the shaved cervical region. To gain access to the cisterna magna, a 1-mm incision was made on the atlanto-occipital membrane between the skull and C1 vertebrae after the targeted membrane area was exposed by surgery. The incision was washed four times with sterile Gibco DPBS 1X (Thermo Fisher, Waltham, MA) to remove excess blood and CSF. A 28G plastic injection cannula (PlasticsOne, Roanoke, VA) was implanted through the incision and secured by tissue glue. As bolus intra-CSF injections have been shown to alter intracranial pressure (ICP) in rodents[36], a small quantity of CSF (≥ 200 µL) was allowed to efflux passively before the intra-CSF injection. For the

ARTICLE IN PRESS

ARTICLE IN PRESS

injection itself, a remote infuse/withdraw dual syringe pump was used to infuse gadoteridol solution (25 mM) at a rate of 5 μL/min for 20 min at a precise depth of 1.0 mm. Upon the completion of infusion, the cannula was left in place for an additional 5 min before removal. The incision was closed using tissue glue and tissue cement. Animals were then transferred to a holder and placed in an MRI scanner for imaging under 1.5% isoflurane for about three hours.

Magnetic resonance imaging

Before and after the procedures conducted outside the scanner, all animals were imaged using 7 T (CSF) or 9.4 T (US and LPA) Biospec MRI scanners (Bruker, Ettlingen, Germany) scanner operating with birdcage transmit and surface receive coils. Relaxation time mapping data were acquired using a RAREVTR (rapid acquisition with relaxation enhancement with variable repetition time) scan with *TR* values of 5000, 3000, 1500, 1000, 500, 250, 150, and 120 ms, with *TE* values of 10, 30, 50, 70, and 90 ms in both the coronal and sagittal planes. A single slice was acquired for each scan sequence, with slice thickness of 1 mm, flip angle of 180°, RARE factor of 2, FOV of 5 x 2.5 cm (sagittal) or 2.5 x 2.5 cm (coronal), and matrix sizes of 150 x 75 (sagittal) or 75 x 75 (coronal). The coronal slice was positioned 5 mm posterior to the dip in the olfactory bulb, and sagittal slices were positioned 2 mm lateral to the midline on both left and right. Throughout imaging, data acquisition alternated among coronal, left sagittal, and right sagittal scans.

MRI data analysis

Images were reconstructed in the Bruker Paravision software, and all subsequent analysis was performed in MATLAB (MathWorks, Natick, MA) using custom scripts. To convert raw T_1-weighted MRI data to R_1 maps, the raw signal intensities at different *TR* values for each voxel were fit to an exponential decay function $S = A(1 - e^{-R_1 TR})$, where S is the measured signal as a function of *TR* for each voxel and A and R_1 are amplitude and relaxation rate parameters, respectively. Voxels for which R_1 values could not be obtained from this procedure, or for which fitted R_1 values were excessively high (> 5 s^{-1}) were excluded from further analysis.

Further analysis was performed using R_1 maps obtained by the procedure described above. Reported R_1 histograms were computed for left sagittal slices, ipsilateral to BBB disruptions created by US and LPA techniques. ΔR_1 values were obtained by subtracting average pre-injection R_1 values from post-injection values for each voxel. Digital ROIs were defined with reference to a rat atlas image 2 mm lateral to the midline[38]. Kinetic analysis was performed using the MATLAB Curve Fitting Toolbox. Individual voxel ΔR_1 time courses were fit using nonlinear least squares to a two compartment model of agent influx and efflux: $\Delta R_1 = \frac{c}{k_{out} - k_{in}}\left(e^{-k_{in}t} - e^{-k_{out}t}\right)$. Fits were only accepted if R^2 was greater than 0.8. When computing the average value of an ROI, individual arimals were only included if greater than 50% of the ROI had fitted values. To assess asymmetry of each technique, we defined a lateralization index as $(R_{1,G}/R_{1,L}) - 1$, where $R_{1,G}$ and $R_{1,L}$ denote the mean R_1 values in the hemispheres with greater and lesser contrast enhancement, respectively, 20-40 minutes after injection. Lateral distance from the transducer in US experiments was defined with respect to the center of the transducer. Statistical tests used in this study are noted throughout the paper, and error bars and error margins reflect SEM over animals, unless otherwise specified.

Histology procedures

To obtain images of the vascular endothelium, 3 untreated rats were anesthetized with 4% isoflurane for 5 minutes, switched to a maintance dose of 1.5%, and injected with 1 mg/mL Texas Red-conjugated tomato lectin (TL, Vector Laboratories) via a tail vein catheter. After 5 minutes,

ARTICLE IN PRESS

rats were transcardially perfused with PBS and 4% paraformaldehyde. 50 uM slices approximately 2 mm from midline were selected for imaging.

To capture the density ZO-1 and LPAR6, 3 untreated rats were perfused with PBS, and the brain tissue was extracted and flash frozen in an isopentane and liquid nitrogen bath for approximately 30 seconds. Brains were transferred to a container pre-chilled on dry ice and then stored at -80° C. For fixation, tissue was then embedded in OCT compound inside a cryomold and stored at -80° C. All were parasagittally sectioned at a cryostat to 14 um thickness. Antibody staining was performed on sections approximately 2 mm from midline. Overnight incubation with primary antibodies was performed at 4C (1:100 dilution, 33-9100 or PA5-115705, Invitrogen). This was followed by 2 hours of secondary incubation (1:500, A28175, Invitrogen) and 10 minutes incubation with 1:2000 Hoechst nuclei stain at room temperature.

The stained brain sections were mounted on glass slides with Invitrogen ProLong Gold Antifade (Fisher Scientific Company) and protected with a coverslip. Fluorescence imaging was performed using a confocal microscope (Axio Imager 2, Zeiss). To assess histological marker density in comparison to features captured by MRI, the histological data was fit to the atlas and downsampled to the resolution of the MRI analysis results.

***In vitro* assessment of LPA activity**

Polydimethylsiloxane-based microfluidic devices were designed and fabricated following established protocols.[29] The devices include one central blood-brain barrier culture channel and two adjacent media channels. Human astrocytes (product #1800 from ScienCell Research Laboratories, Carlsbad, CA) and brain vascular pericytes (ScienCell #1200) were cultured in astrocyte media (ScienCell #1801) and pericyte media (ScienCell #1201), respectively. Green fluorescent protein-expressing human brain microvascular endothelial cells (cAP-0002GFP from Angio-Proteomie, Boston, MA) were cultured in VascuLife (LL-0003 from Lifeline Cell Technology, Frederick, MD) with 10% volume/volume (v/v) fetal bovine serum (FBS). Endothelial cells, pericytes, and astrocytes were seeded at a 6:0.5:1 ratio within a fibrin gel (3 mg/mL) in the central culture channel. Perfusable vessels self-assembled over five days following introduction of a pressure gradient between the two media channels. The seeding medium was made using VascuLife supplemented with 25% heparin sulfate and 2% v/v FBS.

Three LPA models were treated with 150 μM of LPA in culture media and three control models were treated with culture media alone for 15 min before imaging. 40 kDa Texas Red dextran (Thermo Fisher, #D1829) was diluted in culture media at 1:100, and perfused through the vessels with 150 μM of LPA for the LPA models and without LPA for the control models. The dextran perfusion into the surrounding matrix was imaged at 3 min intervals for 30 min or once dextran from the media channel leaked via the fibrin gel into the field of view. Confocal images were acquired using an Olympus FV1200 confocal laser scanning microscope with a 10x objective. Images were analyzed using a custom code in ImageJ[26].[42] Permeability P was calculated during each time interval (3 min) using the following equation:

$$P = \frac{1}{\Delta t} \frac{V_m}{SA_v} \frac{\Delta I_m}{\Delta I}$$

where Δt is the time interval, ΔI_m is the increase in fluorescence intensity in the matrix with volume V_m, SA_v is the surface area of the vasculature, and ΔI is the difference in average intensity between the vasculature and matrix at the beginning of the measurement.

ARTICLE IN PRESS

Statistics and reproducibility

Descriptive and inferential statistical measures are reported throughout the text. Stated sample sizes refer to biological replicates (typically the number of animals), unless otherwise noted. Sample sizes were chosen to ensure replicability and measure effect sizes, rather than on the basis of specific power calculations. Randomization and blinding were not performed, and the study was not preregistered.

Data availability

Processed data are presented in the text, figures, and Supplementary Information. Numerical source data used to generate graphs in this study are provided as an accompanying Supplementary Data file. Raw data for key experiments has been deposited with the Dryad repository at DOI: *10.5061/dryad.tqjq2bwb7*.

Code availability

No substantial code was produced as part of this study.

ARTICLE IN PRESS

ARTICLE IN PRESS

FIGURE CAPTIONS

Figure 1 | Techniques for widespread delivery of small molecules to the brain. a, Positions of coronal (bregma –4 mm) and sagittal (±2 mm lateral to midline) slices used for imaging and R_1 mapping throughout the study. **b,** Schematics of delivery techniques. Left: US delivery combining intravascular delivery of microbubbles via the tail vein (*i*) and transcranial sonication (*ii*), followed by contrast agent injection (*iii*). Middle: LPA-mediated BBB disruption combining contrast agent and LPA (cyan) delivery via the carotid artery (CA, red). Right: Intra-CSF injection of contrast agent into the cisterna magna (CM). **c,** Representative T_1-weighted MRI scans (top) and R_1 maps (bottom, color scale) of individual animals approximately 30 minutes following four treatments. Left to right: control intracarotid injection of gadoteridol, US-mediated BBB disruption, LPA-assisted BBB disruption, and intra-CSF infusion. **d,** Comparison of average R_1 distributions observed in sagittal slices observed following control intracarotid injection (gray, $n = 4$), US delivery (left, $n = 3$), LPA delivery (middle, $n = 5$), and intra-CSF delivery (right, $n = 4$). Vertical dashed lines indicate 2 SD above the mean of IV-injected control animals. Error bars denote SEM over animals within each histogram bin.

Figure 2 | Spatial distribution of contrast enhancements after molecular delivery. a, Mean (left) and standard deviation (right) maps of R_1 values measured ~30 minutes after treatment with the three delivery techniques or control injection. **b,** Anatomical divisions used for ROI analysis. Abbreviations: brainstem (BS), cerebellum (Cb), corpus callosum (cc), cortex (Cx), dorsal striatum (dSt), hippocampus (Hi), hypothalamus (HT), midbrain (MB), thalamus (Th), ventral striatum (vSt), whole brain (WB). **c,** Quantification of contrast enhancements (ΔR_1 values) by ROI for each of the treatment conditions. Horizontal lines depict mean values and dots represent results from individual animals. **d,** Correspondence of mean R_1 changes reflecting brain delivery after LPA and US treatments. Dashed line denotes linear regression result. **e,** Correspondence of R_1 changes after LPA and CSF injection methods. Error bars in **d** and **e** denote SEMs over animals.

Figure 3 | Molecular transport after brain delivery. a, R_1 values over time, following contrast agent delivery in conjunction with the four treatment conditions indicated. Error bars denote SEMs. **b,** Times to peak contrast enhancement following US-mediated delivery, LPA-based administration, and intra-CSF infusion techniques. Dots represent individual animals, horizontal lines show mean values (US $n = 3$, LPA $n = 5$, CSF $n = 4$). **c,** Voxel-level modeling used to estimate washout rates for each voxel in each sagittal R_1 time course. Individual voxels are represented by MRI time courses (gray) with fitted curves (magenta) superimposed for voxels where curve fitting was successful. Inset shows a representative fit to data from one voxel in one animal treated with LPA. **d,** Maps showing average k_{out} values (color scale; gray denotes unfit voxels) from animals treated with US, LPA, and CSF delivery techniques. **e,** Quantification of washout rates over ROIs. Gray rectangles denote regions for which average rates could not be obtained from two or more animals. Dots represent individual animals, horizontal lines show mean values. **f,** Comparison of mean k_{out} values measured following LPA, US, and CSF delivery. Dots represent means and error bars represent SEMs of 2-5 animals for which ROI-specific mean data from both compared techniques was available.

Figure 4 | Histological correlates of brain delivery results. a, Visualization of vascular endothelial cells using tomato lectin (TL) staining in a representative brain sagittal slice. **b,**

ARTICLE IN PRESS

Visualization of the tight junction marker ZO-1. **c,** Visualization of staining for the LPA receptor LPAR6. Closeups in **a-c** correspond to regions denoted by dotted rectangles, with corresponding scale bars: 2 mm (top), 500 µm (bottom left), 200 µm (bottom right). **d,** Average relative fluorescence intensities (color scale, all $n = 3$) from brains stained with TL, anti-ZO-1, and anti-LPAR6, represented with the geometry and resolution of corresponding sagittal MRI scans. **e,** Quantification of histological results over ROIs. Dots represent individual animals, horizontal lines show mean values. **f,** Correlation coefficients (left) and corresponding –log(p) values for ROI-level comparisons between average ΔR_1 values (post-US, LPA, and CSF) and mean histological staining intensities (TL, ZO-1, and LPAR6). Green outline denotes $p \leq 0.05$ ($n = 10$ ROIs). **g,** Qualitative comparison between delivery technique assessed in this study. Larger circles denote comparatively greater values for each of the criteria.

Editorial Summary:
Parallel characterization of three techniques for brain-wide delivery of a BBB-impermeable molecule indicates comparative strengths and weaknesses of each method, while suggesting mechanistic contributions to delivery efficiency.

Peer Review Information:
Communications Biology thanks Bilal syed Nizami and the other, anonymous, reviewer(s) for their contribution to the peer review of this work. Primary Handling Editors: Adib Keikhosravi and Benjamin Bessieres. A peer review file is available.

ARTICLE IN PRESS

ARTICLE IN PRESS

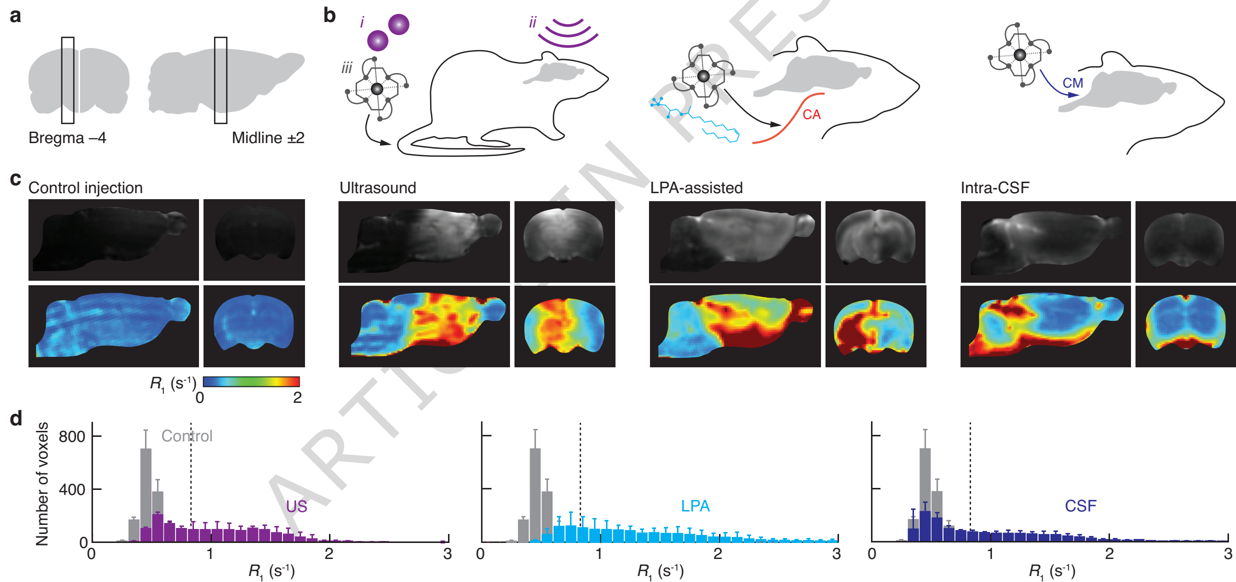

ARTICLE IN PRESS

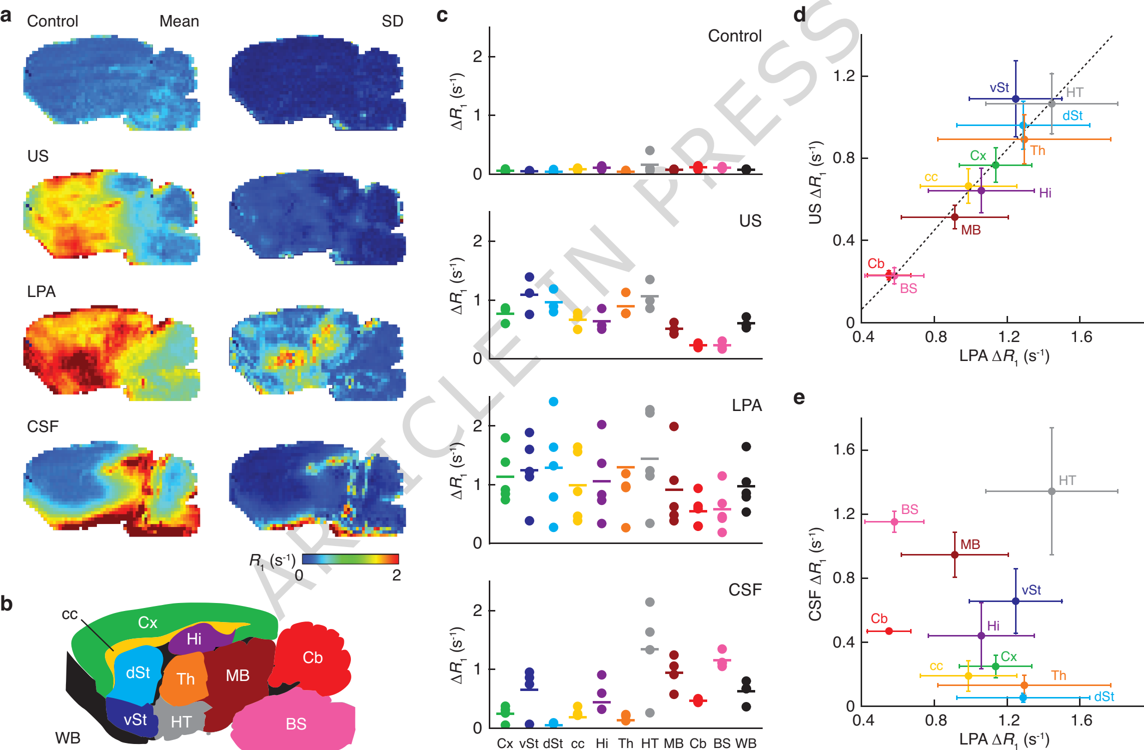

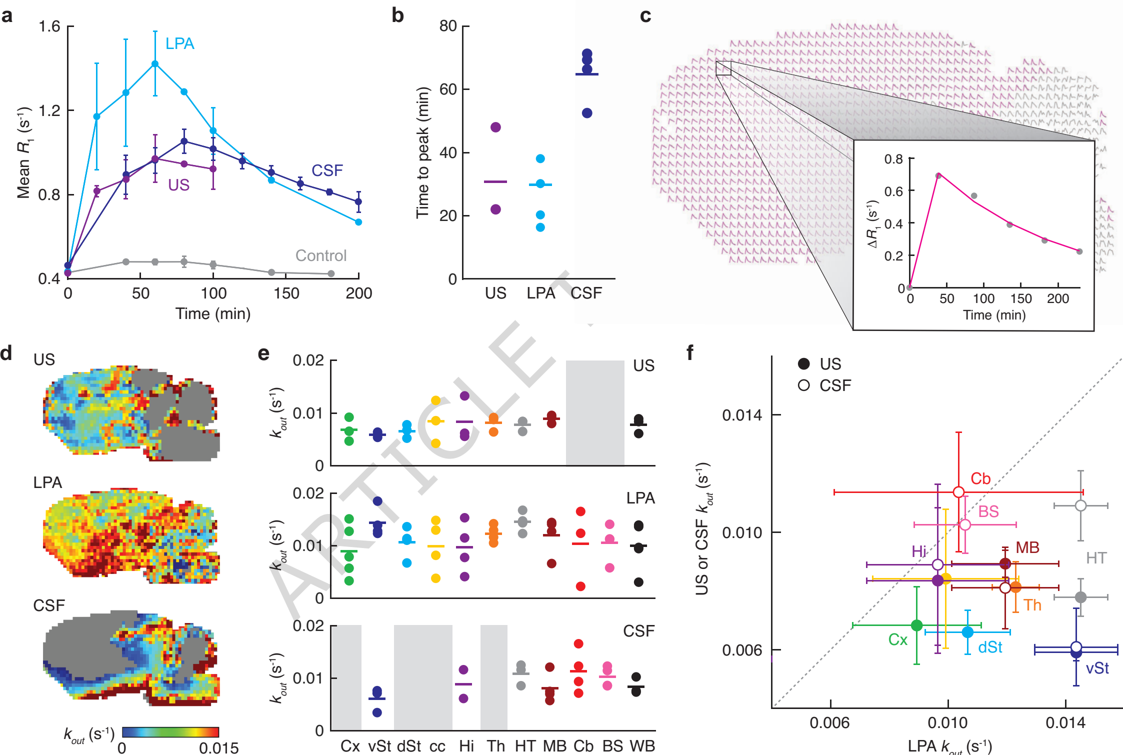

ARTICLE IN PRESS

ARTICLE IN PRESS